Chinese Chemical Letters 35 (2024) 109877

Contents lists available at ScienceDirect

Chinese Chemical Letters

journal homepage: www.elsevier.com/locate/cclet

Promoting exciton dissociation by metal ion modification in polymeric carbon nitride for photocatalysis

Yue Pan[a], Wenping Si[b,*], Yahao Li[a], Haotian Tan[a], Ji Liang[a,*], Feng Hou[a,*]

[a] Key Laboratory of Advanced Ceramics and Machining Technology, Ministry of Education, School of Materials Science and Engineering, Tianjin University, Tianjin 300072, China
[b] School of Material Science and Engineering, Hebei University of Technology, Tianjin 300130, China

ARTICLE INFO

Article history:
Received 18 January 2024
Revised 7 April 2024
Accepted 8 April 2024
Available online 9 April 2024

Keywords:
Exciton dissociation
Carbon nitride
Photocatalysis
Alkali metal ions
Exciton binding energy

ABSTRACT

Carbon nitride, a typical low-dimensional conjugated polymer photocatalyst, features a high exciton binding energy due to the weak dielectric screening and the strong Coulombic attraction of photogenerated electrons and holes. The reduction of the exciton binding energy of carbon nitride to promote the conversion from excitons into free carriers is the first priority for the improvement of charge-transfer-dependent photocatalytic reaction activity. In this paper, by introducing a variety of polar metal cations to carbon nitride, it is demonstrated that the charge distribution of the heptazine ring can be improved by ion polarization, which effectively promotes the dissociation of excitons into electrons and holes. The sodium ion shows the best modification effect, which enhances the rate of both photocatalytic hydrogen and hydrogen peroxide production by about 50%. Characterization shows that the introduction of strongly polar metal cations contributes to the reduction of the exciton dissociation energy of carbon nitride. This study provides a new perspective and a convenient method for the exciton modulation engineering of low-dimensional photocatalysts.

Energy shortage and environmental pollution have raised an unprecedented urgency on clean and renewable energy supplies [1–3]. Light energy conversion using semiconductor-based photocatalysts attracts great interest in energy and environment concerns. Carbon nitride (CN), due to its suitable band edge positions and easy accessibility, is able to be excited by photons for the generation of oxidation and reduction centers to catalyze many reactions driven by charge transfer, such as photocatalytic hydrogen and hydrogen peroxide production [4–13].

At present, energy band structure optimization and charge separation are recognized as general strategies for regulating carrier production in CNs, but photocatalysts generate both excitons and free carriers when excited by light, and excitons can be dissociated into free carriers [5,6,14,15]. Therefore, it is necessary to take the competitive excitons into account. Actually, excitons are bound-state electron-hole pairs combined by the long-range Coulomb interaction. The electric field lines joining the electron and hole in excitons extend widely into the surrounding dielectric, which can respond significantly to changes in the dielectric environment within a few nanometers of the material [16–19]. In the limit of atomically thin materials, the electrons and holes forming excitons are strongly confined to the plane of the monolayer. Consequently, the electric field lines joining the electrons and holes begin to extend outside of the sample and additionally experience weaker screening due to the change in the dielectric environment [20–22]. Therefore, compared with inorganic bulk phase semiconductor photocatalysts, two-dimensional carbon nitride nanosheets (CNN), as a typical low-dimensional conjugated polymer, are subject to weak dielectric screening of photoexcited electron-hole pairs in the two-dimensional limit. The strong Coulombic interactions between the electrons and the holes leads to a larger obstacle in the dissociation of excitons into free carriers which can be quantified as a sharp increase in exciton binding energy (E_b) [23–25]. The low concentration of free carriers associated with the high E_b is unfavorable for carrier-induced and charge-transfer-dependent photocatalytic reactions, which results in the limitation of the intrinsic photocatalytic performance of two-dimensional CNN.

In order to enhance the photocatalytic performance of CN, it is necessary to reduce E_b by modulating the dielectric environment to facilitate the dissociation of excitons into free carriers. The dielectric constants of organic semiconductors are related to multi-polarization contributions such as electron, atom/vibration, orientation/dipole and ion polarization. Therefore, polarization engineering, for example, the introduction of polar ions [12,15,26,27] or

* Corresponding authors.
E-mail addresses: siwp@hebut.edu.cn (W. Si), liangji@tju.edu.cn (J. Liang), houf@tju.edu.cn (F. Hou).

https://doi.org/10.1016/j.cclet.2024.109877
1001-8417/

groups [28], has been confirmed to be effective in increasing the dielectric constant and regulating E_b and exciton energy gaps. This strategy can modulate the charge distribution of the polymer, improve the dielectric shielding in the electron- hole pair and substantially decrease the E_b of CN.

Based on the above considerations, we introduce typical metal cations without intrinsic electrocatalytic activity, such as lithium, sodium, potassium, calcium and magnesium ions into CNN by a solvothermal method to regulate the charge distribution of carbon nitride without changing the electrocatalytic activity of materials. This strategy significantly modulates the dielectric environment of CNN at the atomic scale and lowers the E_b, thus promoting exciton dissociation into free carriers and resulting in higher photocatalytic performance. With the modification of metal cations, the exciton dissociation energies of the photocatalyst are decreased. Among them, sodium ions exhibit the most evident effect, resulting in a great reduction in E_b and significant increase in the carrier ratio. As a consequence, the rates of both the photocatalytic hydrogen evolution reaction (HER) and the photocatalytic synthesis of hydrogen peroxide by carbon nitride nanosheets with sodium ions introduced (NaCNN) are increased by 50% compared with that of CNN. This paper describes the strong correlation between the dielectric environment and exciton dissociation in the carbon nitride in detail, which provides a new perspective for the exciton regulation engineering of low dimensional photocatalysts.

In this research, DCDA-DI water solution was freeze-dried into a white sponge-like complex network composed of nanostructured flakes. The nanostructured DCDA was subsequently calcined to form BCN. The as-prepared BCN was dispersed in an IPA-DI water solvent mixture, which was sonicated and then added to an autoclave to synthesize ultrathin CNN by solvothermal treatment, as shown in Fig. S1 (Supporting information). The nanosheets are crumpled and buckled at the edges due to the repulsion between the lone pair electrons of the terminal nitrogen atoms [29]. Meanwhile, the abundant in-plane wrinkles caused by ultrasonic treatment indicate the introduction of tension strain effect, which contributes to the enhancement of the steady-state optical transition [30,31]. Ultrasonication-assisted liquid phase exfoliation and solvent-thermal assisted exfoliation were combined to obtain CNN, resulting in ultra-high specific surface area and exposure of more photocatalytic active sites [8,32-34]. Metal ion-modified CNN was obtained through the same two-step ultrasonication and solvent-thermal treatment of BCN. We examined that there is almost no change in the H_2 evolution rate when the salt concentration is higher than 5 mmol/L. Therefore, the modified CNN were prepared with 5 mmol/L salt solutions and investigated (Fig. S2 in Supporting information). As shown in Figs. S3–S6 (Supporting information), it is demonstrated that the morphology of the carbon nitride modified by metal cations still remain as multi-pleated ultrathin nanosheets. Due to the low doping concentration, there is no presence of any embedded particles on the carbon nitride nanosheets. However, the presences of C, N, O and the corresponding metal elements (Li, Na, K, Mg and Ca, respectively) are confirmed in the structures of the CNN modified with different metal ions as shown in Figs. 1a and Figs. S7–S10 (Supporting information). In particular, the metal elements can be detected throughout the entire structure of each sample, respectively, verifying the introduction and homogeneous dispersion of the metal elements in the CNN.

The XRD patterns of the different samples are provided in Fig. 1b. As shown, CNN, LiCNN and NaCNN all exhibit (210) and (002) diffraction peaks at 12.7° and 27.6°, which are associated with the in-plane repeating motif of the aromatic system and the interlayer stacking reflection of the graphite structure, respectively [29,35,36]. This suggests that the nanosheet structure of CNN was well preserved after the introduction of metal cations, which is consistent with the observation of TEM images. It is observed that

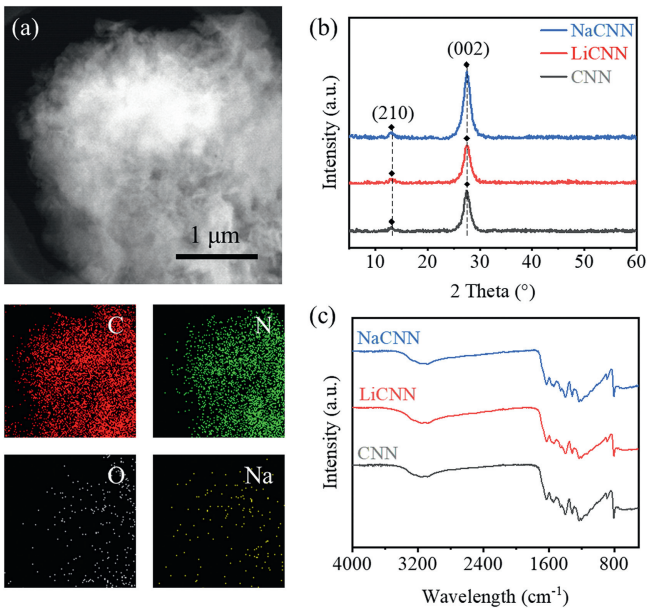

Fig. 1. (a) HADDF-STEM and corresponding EDS mapping of C, N, O and Na elements in NaCNN. (b) XRD patterns and (c) FTIR spectra of CNN, NaCNN and LiCNN.

the half peak width of the (002) peak of NaCNN increases obviously, indicating that the modification of the metal cation causes the smaller interlayer spacing of carbon nitride [37]. The reduction of the interlayer spacing promotes charge transfer through the interlayer and from the bulk to the interface [38], and verifies the attraction of the metal cation to the heptazine ring with negative charge distribution. As seen from the FTIR spectra in Fig. 1c, the absorption peaks of the metal cation modified LiCNN and NaCNN are also similar to those of CNN, which is consistent with the XRD results. Specifically, the sharp peak at around 810 cm^{-1} is ascribed to the typical breathing vibration of triazine modes, and the characteristic absorption peaks in the wide spectral band range at 1200−1600 cm^{-1} correspond to the stretching vibration of the aromatic heterocyclic ring in the carbon nitride [39–41], confirming the heptazine unit-based carbon nitride structures for CNN with and without metal cations. The wide absorption band at the region of 2900−3400 cm^{-1} is attributed to the residual N–H and O–H components from the uncondensed amino groups and surface adsorbed H_2O molecules [42], which does not distinguish significantly between the different samples. These results demonstrate that the introduction of metal cations does not alter the structure of CNN.

To further investigate the effect of modification on carbon nitride, the surface chemical composition and electronic states of carbon nitride were measured by XPS spectroscopy. As shown in Fig. S11 and Table S1 (Supporting information), C, N, O, and respective metals can be recognized in the survey spectra of the LiCNN and NaCNN [43]. A few oxygen atoms may originate from the polymerization process of CNN and from water and isopropanol. The peak of chlorine is not observed in these samples, probably because of the relatively large ionic radius of Cl^- or being ion exchanged with hydroxyl groups (Fig. S12 in Supporting information) [44,45]. High-resolution XPS spectroscopy indicates that LiCNN (Fig. S13 in Supporting information) and NaCNN (Fig. S14 in Supporting information) exhibit typical Li 1s and Na 1s signals at 53.6 eV and 1071.5 eV, respectively, which confirms that both Li^+ and Na^+ have been successfully introduced into the CNN structure in consistence with the EDS results [43]. As shown in Fig. 2a, The C 1s peak of CNN can be deconvoluted into three peaks at about 284.8, 286.2, and 288.2 eV, which is caused by amorphous

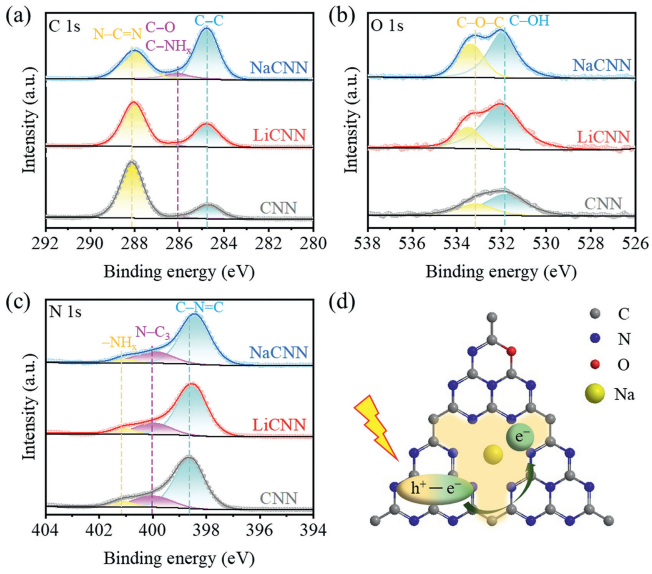

Fig. 2. High-resolution XPS spectra of CNN, LiCNN, NaCNN: (a) C 1s, (b) O 1s and (c) N 1s. (d) Schematic representation of exciton dissociation and charge-dependent reaction of NaCNN.

carbon at the edge of the heptazine ring, C–NH_x ($x = 1, 2$) or C–O, and N–C=N coordination in the CNN framework, respectively. The peak area occupancy of the C–NH_x groups ($x = 1, 2$) of NaCNN and LiCNN increases compared to that of pristine CNN, accompanied with a slight shift of the peaks toward higher binding energies. This phenomenon corresponds to the disruption of C=N group by hydroxyl attack to form the C–O group and is favored in the O 1s spectra (Fig. 2b). The OH peak at 531.8 eV changes a little, but the significant increase in the area occupancy of the C–O–C peak at 533.2 eV indicates that the metal cation modification introduces more O atoms into the CNN framework [43,46,47].

The high-resolution N 1s spectra of CNN (Fig. 2c) shows peaks at 398.7 eV, 400.0 eV, and 401.3 eV, corresponding to bi-coordinated N in the C–N=C group, tri-coordinated N atoms in N–$(C)_3$, and the amino-functional group (C–NH_x), respectively. After Li^+ and Na^+ modification, the peak area occupancies of the three N 1s peaks are almost unchanged, but the peak positions are shifted towards lower binding energies because of an increase in the electron density of N atoms. The electron transfer can be attributed to the fact that the overlap of the electron shells are formed between the polar metal cations and their surrounding nitrogen atoms with lone electron pairs [45,48]. As shown in Fig. S15 (Supporting information) and Fig. 2d, this change in charge distribution alters the extraction of electrons from the local structure. Meanwhile, it is demonstrated that the metal cations are captured by the traps consisting of heptazine rings (diameter of about 0.477 nm, which is larger than the ionic diameters of Na (0.102 nm) and Li (0.076 nm) [44,47]. Comparing NaCNN and LiCNN, it is observed that the shift of binding energy peak position of NaCNN is more significant than that of LiCNN. It is because Na^+ is more polarizable than Li^+ and has a larger overlap area with the electronic shell of the CNN, thus provides a better ionic polarization effect on the CNN [49]. Therefore, NaCNN has a more positive charge distribution in the heptazine ring, stronger pull on the electrons and thereby a much lower exciton binding energy, which is more favorable for the separation of electrons and holes.

^{13}C NMR spectroscopy measurement was performed to further identify the chemical structure of the samples (Fig. S16 in Supporting information). The characteristic peaks at 157 and 165 ppm for CNN relate to the C atoms in CN_2–(NH_2) and CN_3 groups [50,51], respectively, indicating the formation of tri-*s*-triazine rings in the carbon nitride framework. For NaCNN, the signals of CN_2–(NH_2) and CNN are shifted to higher field. Meanwhile, the CN_3 signal is splitted into two peaks at 167 ppm and 172 ppm. It can be explained that the interaction between Na^+ ions and the heptazine ring leads to an increase in the electron density of the heptazine ring [51]. From the ^{23}Na NMR spectrum, it can be observed that Na is successfully doped into the carbon nitride framework [52]. This result is consistent with the XPS analysis.

Subsequent Mott–Schottky measurements were performed to determine the flat band potentials of CNN and NaCNN. As shown in Fig. S17 (Supporting information), the Mott-Schottky plots of these samples all exhibit positive slopes, indicating the n-type semiconductor nature [53]. For n-type semiconductors, the flat band potential can be approximated as the conduction band minimum (CBM). Therefore, the CBM values of CNN and NaCNN can be determined as −0.79 and −0.66 eV, respectively, from the intersection of the tangent line with the x-axis.

On this basis, the band gap and optical absorption of the materials were investigated by UV–vis diffuse reflectance spectroscopy (UV-DRS). The absorption intensity and response range of NaCNN in the visible region are very similar to those of CNN (Fig. S18 in Supporting information). According to the corresponding Tacu plots (Fig. S19 in Supporting information), the band gaps of CNN, NaCNN are calculated to be 2.693 and 2.691 eV, respectively. It is observed that the metal cation modification has negligible effect on the band gap and light absorption properties of CNN. The AQE values of H_2 evolution on CNN, LiCNN and NaCNN under 400 nm, 420 nm and 500 nm illumination are shown in Fig. S20 (Supporting information). The change tendency of AQE value is in accord with the light absorption spectrum.

The electron-hole recombination efficiency of CNNs and metal ion modified CNN are further evaluated by photoluminescence (PL) measurements. As shown in Fig. S21 (Supporting information), excited by 369 nm light, CNN, LiCNN, and NaCNN all exhibit photoluminescence at 468 nm. Note that the intensities of the normalized PL peaks are consistent for all three samples, which indicates that the introduction of polar cations does not change the concentration of excitons generated by photons. In order to further reveal the mechanism of the faster separation of electrons and holes as well as the competition of free carrier and exciton effects in the metal cation-modified CNNs, the E_b values of CNN, LiCNN, and NaCNN were measured by temperature-dependent photoluminescence. The integrated PL intensity decreased with temperature increasing (Figs. 3a–c). The E_b was calculated by fitting the integrated PL emission as a function of temperature according to Arrhenius equation, *i.e.*, $I(T) = I_0/(1 + A\exp(-E_b/(k_BT)))$ [26,28]. Compared with CNN, both LiCNN and NaCNN show a slight decrease in E_b. Na^+ modification leads to the largest decrease in E_b from 74 meV for CNN to 66 meV for NaCNN. These results indicate that the introduction of polar ions can modulate the dielectric environment of CNN, and the more polarizable Na^+ contributes to a more positive local charge distribution through ion-dipole interactions, which greatly facilitates the dissociation of excitons and enhances the charge-carrier-induced photochemical reactions.

The *in-situ* electron spin resonance (ESR) technique was employed to confirm the above conclusions. The DMPO was utilized to quench $^{\bullet}O_2^-$ in the aerobic condition of water. As shown in Fig. 3d, the DMPO signal intensity of the three samples increases instantaneously and dramatically under light irradiation, which suggests that a large number of electrons are generated from the separation of strongly bound excitons and utilized in the single electron reduction from O_2 molecules to $^{\bullet}O_2^-$ [54]. Moreover, the order of magnitude of the growth of the DMPO signal intensity under illumination is CNN < LiCNN < NaCNN. It is visually demonstrated

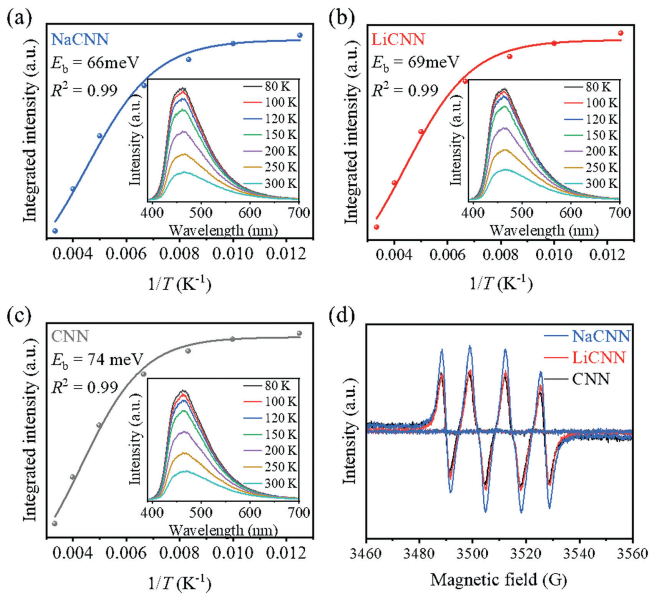

Fig. 3. Integrated PL emission intensity of (a) NaCNN, (b) LiCNN and (c) CNN as a function of temperature fitted by Arrhenius equation (inset is the temperature-dependent PL spectra). (d) DMPO-trapped *in-situ* ESR of NaCNN, LiCNN and CNN.

that polar metal cation doping contributes to the production of more photogenerated electrons. With the same exciton concentration of three samples, polarmetal cation contributes to the dissociation of more excitons into more free electrons for charge-induced photochemical reactions. More importantly, the stronger the polarity of the metal cation, the more significant the polarization effect to promote exciton dissociation.

Photocatalytic hydrogen evolution reaction (HER) is a typical charge transfer dependent photochemical reaction and a promising approach for the future production of sustainable chemical fuels. In this paper, it is used to characterize the photocatalytic activity of carbon nitride with different exciton binding energies. The photocatalytic hydrogen evolution reaction in the presence of carbon nitride was carried out using TEOA as hole scavenger and Pt (3 wt%) as co-catalyst. Under light irradiation, the formation of H_2 is observed over the employed photocatalysts with a linear time-dependent increasing concentration (Fig. S22 in Supporting information). As shown in Fig. 4a, the photocatalytic HER rates for LiCNN and NaCNN are 5771 μmol g^{-1} h^{-1} and 6375 μmol g^{-1} h^{-1}, respectively. In particular, NaCNN shows the highest HER rate, which is higher than that of CNN (4050 μmol g^{-1} h^{-1}) by 57.4%. Moreover, the cycle stability of samples was also tested and the results are shown in Fig. 4b and Fig. S23 (Supporting information). In the case of NaCNN, for example, HER rate reduces by only 5% after five cycles of the photocatalytic process and remains above 4050 μmol g^{-1} h^{-1}. More importantly, CNN modified with polar metal cations can also better drive other charge-transfer dependent photocatalytic reactions, such as hydrogen peroxide (H_2O_2) production. The photocatalytic production of H_2O_2 was carried out in an O_2-saturated environment using isopropanol as the hole scavenger. As shown in Fig. S24 (Supporting information) and Fig. 4a, the photocatalytic production rates of H_2O_2 by LiCNN and NaCNN are 1491 μmol g^{-1} h^{-1} and 1669 μmol g^{-1} h^{-1}, respectively. It is similar to the increase in the HER rates that NaCNN shows the highest rate which is higher than that of CNN (1032 μmol g^{-1} h^{-1}) by 61.7%. NaCNN also shows excellent photocatalytic stability in the photocatalytic production of H_2O_2 (Fig. 4b). Meanwhile, NaCNN holds multi-pleated structure and interlayer spacing after long time photocatalysis (Fig. S25 in Supporting information). In conclusion, CNN modified by metal cations reached a decent level of photocatalytic performance compared to literature reports (Tables S2 and S3 in Supporting information) [54–61].

Furthermore, electrochemical methods were used to reveal the kinetic process of photogenerated exciton separation. On the one hand, the transient photocurrent response tests shows that the transient photocurrent responses of CNN, LiCNN, and NaCNN enhance successively (Fig. S26 in Supporting information) [62–64]. On the other hand, electrochemical impedance spectroscopy (EIS) was measured to further understand the effect of polar metal cation modification on the charge transfer process at the CNN/electrolyte interface. The electrodes in the test system exhibited bulk transport resistance R_{bulk} and photoelectrode-electrolyte charge transfer resistance R_{ct}. R_{ct} and $(RC)_{ct}$ describe the difficulty and rate of charge transfer, respectively. As shown in Fig. 4c, the diameter of the semicircle in the high frequency field is in the sequence NaCNN < LiCNN < CNN, demonstrating that the introduction of polar metal cations promotes the exciton dissociation efficiency and carrier mobility [65]. By fitting the Nyquist diagram with the equivalent circuit shown in Fig. S27 (Supporting information), it is demonstrated that R_{ct} and $(RC)_{ct}$ at the solid-electrolyte interface are both ordered as follows: NaCNN < LiCNN < CNN. It is confirmed that the introduction of polar metal cations into CNN electrodes promotes the surface OER kinetics, which is consistent with the transient photocurrent response [66]. These results indicate that the higher the polarizability of the introduced metal ions, the larger the overlap area with the electron shell of CNN. In other words, with the effect of ion-dipole interactions, CNN modified by metal ions with high polarizability has a more positive charge distribution than CNN. Combined with the schematic diagram of Fig. 4d, the photophysical model of exciton dissociation can be described as follows: The electrons transfer from the conduction band to the trap state and form excitons, and the formed excitons overcomes the E_b to dissociate into free charges [67]. The modified surrounding dielectric environment leads to a decrease in E_b, which is favorable for the separation of

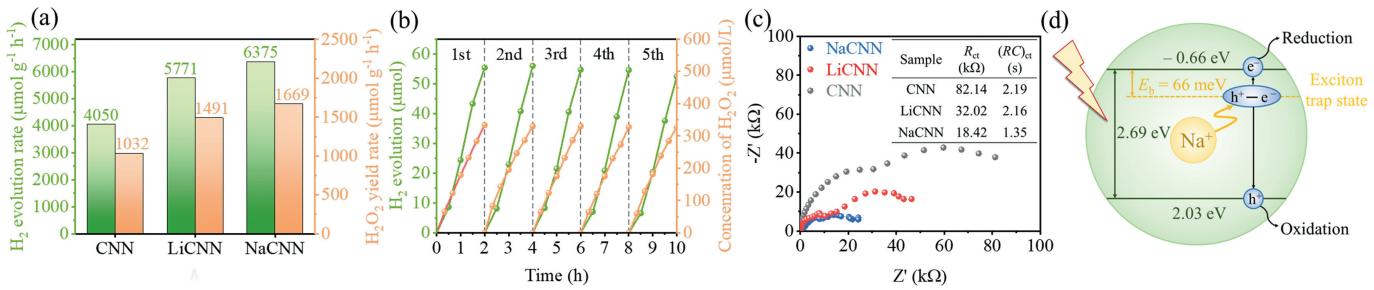

Fig. 4. (a) Photocatalytic H_2 evolution and H_2O_2 production rates of NaCNN, LiCNN and CNN. (b) Cycling stability of NaCNN for photocatalytic H_2 evolution and H_2O_2 production. (c) Nyquist plots for NaCNN, LiCNN and CNN. Inset: The charge transfer resistance (R_{ct}) and time constant $(RC)_{ct}$ at the solid–electrolyte interface obtained by fitting the impedance spectroscopy data. (d) Possible photocatalytic process of exciton dissociation in NaCNN.

photogenerated electrons and holes and thus the improvement of the photocatalytic performance of carbon nitride.

In conclusion, typical metal cations without intrinsic catalytic activity are introduced into CNN by a solvothermal method to modulate the dielectric environment of carbon nitride. Strongly polar metal cations can contribute to a more positive local charge distribution of the heptazine ring through ionic dipole interactions, accompanied by the reduction of the exciton binding energy and the promotion of the dissociation of photogenerated excitons into free electrons and holes, which participate in the charge transfer-dependent photocatalytic reactions. The results indicate that the photocatalytic hydrogen and hydrogen peroxide production rate of NaCNN, which exhibits the lowest E_b, are both increased compared to those of CNN. This study provides a convenient method to modulate the dielectric environment of polymer photocatalysts for the regulation of exciton effects and the related photocatalytic behavior.

Declaration of competing interest

The authors declare that they have no known competing financial interests or personal relationships that could have appeared to influence the work reported in this paper.

CRediT authorship contribution statement

Yue Pan: Data curation, Writing – original draft, Investigation, Methodology. **Wenping Si:** Conceptualization, Supervision, Writing – review & editing, Funding acquisition, Investigation. **Yahao Li:** Data curation, Investigation. **Haotian Tan:** Investigation, Methodology. **Ji Liang:** Funding acquisition. **Feng Hou:** Funding acquisition, Writing – review & editing.

Acknowledgment

This work is supported by the National Natural Science Foundation of China (Nos. 22002107, 21905202, 22179093).

Supplementary materials

Supplementary material associated with this article can be found, in the online version, at doi:10.1016/j.cclet.2024.109877.

References

[1] T.R. Cook, D.K. Dogutan, S.Y. Reece, et al., Chem. Rev. 110 (2010) 6474–6502.
[2] X.C. Wang, K. Maeda, A. Thomas, et al., Nat. Mater. 8 (2009) 76–80.
[3] D.M. Schultz, T.P. Yoon, Science 343 (2014) 985.
[4] T. Hisatomi, J. Kubota, K. Domen, Chem. Soc. Rev. 43 (2014) 7520–7535.
[5] H. Wang, S.L. Jiang, S.C. Chen, et al., Chem. Sci. 8 (2017) 4087–4092.
[6] H. Wang, S. Jiang, S. Chen, et al., Adv. Mater. 28 (2016) 6940–6945.
[7] T. Zhang, E. Olsson, M. Choolaei, et al., Materials 13 (2020) 32143293.
[8] Y.H. Wang, L.Z. Liu, T.Y. Ma, et al., Adv. Funct. Mater. 31 (2021) 2102540.
[9] J. Liu, W. Peng, Y. Li, et al., Trans. Tianjin Univ. 26 (2020) 149–171.
[10] T. Yu, Z. Liu, J. Ma, et al., Trans. Tianjin Univ. 26 (2019) 40–48.
[11] J. Xiao, J. Zhang, L. Pan, et al., Trans. Tianjin Univ. 27 (2021) 280–294.
[12] Y. Zhang, L. Ran, Z. Li, et al., Trans. Tianjin Univ. 27 (2021) 348–357.
[13] Y. Tian, Y. Zong, Y. Zhou, et al., Trans. Tianjin Univ. 27 (2020) 42–54.
[14] P. Zhang, L. Li, J. Zhao, et al., Precis. Chem. 1 (2023) 40–48.
[15] Y. Qian, D. Li, Y. Han, et al., J. Am. Chem. Soc. 142 (2020) 20763–20771.
[16] L.V. Keldysh, JETP Lett. 29 (1979) 658.
[17] J. Deslippe, M. Dipoppa, D. Prendergast, et al., Nano. Lett. 9 (2009) 1330–1334.
[18] E. Hanamura, N. Nagaosa, Mater. Sci. Eng. B 3–4 (1988) 255–258.
[19] K. Tanaka, T. Takahashi, T. Kondo, et al., Phys. Rev. B 71 (2005) 045312.
[20] A. Chernikov, T.C. Berkelbach, H.M. Hill, et al., Phys. Rev. Lett. 113 (2014) 076802.
[21] N.C. Giebink, G.P. Wiederrecht, M.R. Wasielewski, et al., Phys. Rev. B 83 (2011) 195326.
[22] A.I. Hochbaum, P.D. Yang, Chem. Rev. 110 (2010) 527–546.
[23] L.Q. Tian, W.J. Xie, X.X. Wu, et al., J. Phys. Chem. C 124 (2020) 24667–24676.
[24] E.Da Como, Unconventional Thin Film Photovoltaics, Royal Society of Chemistry, Cambridge, 2016.
[25] V. D'Innocenzo, G. Grancini, M.J.P. Alcocer, et al., Nat. Commun. 5 (2014) 3586.
[26] G. Li, P. Fu, Q. Yue, et al., Chem. Catal. 2 (2022) 1734–1747.
[27] G. Liu, H. Lv, Y. Zeng, et al., Trans. Tianjin Univ. 27 (2021) 139–146.
[28] G. Chen, Z.D. Zhang, Y.X. Liao, et al., Small 17 (2021) e2100698.
[29] A. Thomas, A. Fischer, F. Goettmann, et al., J. Mater. Chem. 18 (2008) 4893–4908.
[30] Z.X. Gan, L.Z. Liu, P.F. Pan, et al., Nanoscale 10 (2018) 22448–22455.
[31] H. Tan, W. Si, W. Peng, et al., Nano Lett. 23 (2023) 10571–10578.
[32] Q. Han, B. Wang, J. Gao, et al., ACS Nano 10 (2016) 2745–2751.
[33] Y.T. Xiao, G.H. Tian, W. Li, et al., J. Am. Chem. Soc. 141 (2019) 2508–2515.
[34] S.B. Yang, Y.J. Gong, J.S. Zhang, et al., Adv. Mater. 25 (2013) 2452–2456.
[35] J.S. Zhang, M.W. Zhang, G.G. Zhang, et al., ACS Catal. 2 (2012) 940–948.
[36] E. Alwin, W. Nowicki, R. Wojcieszak, et al., Dalton Trans. 49 (2020) 12805–12813.
[37] Z. Chen, Y. Bu, L. Wang, et al., Appl. Catal. B 274 (2020) 119117.
[38] G. Zhang, G. Li, Z.A. Lan, et al., Angew. Chem. Int. Ed. 56 (2017) 13445–13449.
[39] Y.Y. Lei, W.P. Si, Y.Q. Wang, et al., ACS Appl. Mater. Interfaces 15 (2023) 6726–6734.
[40] Q.H. Liang, Z. Li, Z.H. Huang, et al., Adv. Funct. Mater. 25 (2015) 6885–6892.
[41] P. Niu, L.L. Zhang, G. Liu, et al., Adv. Funct. Mater. 22 (2012) 4763–4770.
[42] Y.P. Zhu, T.Z. Ren, Z.Y. Yuan, ACS Appl. Mater. Interfaces 7 (2015) 16850–16856.
[43] Jigyasa, Pratibha, J.K. Rajput, J. Electroanal. Chem. 878 (2020) 114605.
[44] X. Qu, S. Hu, J. Bai, et al., J. Mater. Sci. Technol. 34 (2018) 1932–1938.
[45] H. Gao, S. Yan, J. Wang, et al., Phys. Chem. Chem. Phys. 15 (2013) 18077–18084.
[46] J. Ma, D. Jin, Y. Li, et al., Appl. Catal. B 283 (2021) 119520.
[47] H. Tang, Z. Xia, R. Chen, et al., Chem. Asian J. 15 (2020) 3456–3461.
[48] A. Kumar, S. Kashyap, M. Sharma, et al., Chemosphere 287 (2022) 131988.
[49] D.A. McQuarrie, J.D. Simon, Physical Chemistry: A Molecular Approach, University Science Books, Sausalito, 1997.
[50] L. Muniandy, F. Adam, A.R. Mohamed, et al., Appl. Surf. Sci. 398 (2017) 43–55.
[51] M.H. Vu, C.C. Nguyen, T.O. Do, ChemPhotoChem 5 (2021) 466–475.
[52] J. Gryko, P.F. McMillan, O.F. Sankey, Phys. Rev. B 54 (1996) 3037–3039.
[53] Y. Lei, W. Si, Y. Wang, et al., ACS Appl. Mater. Interfaces 15 (2023) 6726–6734.
[54] X. Li, W. Bi, L. Zhang, et al., Adv. Mater. 28 (2016) 2427–2431.
[55] J. Meng, Z. Lan, T. Chen, et al., J. Phys. Chem. C 122 (2018) 24725–24731.
[56] N. Ding, L. Zhang, M. Hashimoto, et al., J. Colloid Interface Sci. 512 (2018) 474–479.
[57] V.W.H. Lau, V.W.Z. Yu, F. Ehrat, et al., Adv. Energy Mater. 7 (2017) 1602251.
[58] H. Fattahimoghaddam, T. Mahvelati-Shamsabadi, B.K. Lee, ACS Sustain. Chem. Eng. 9 (2021) 4520–4530.
[59] H.I. Kim, Y. Choi, S. Hu, et al., Appl. Catal. B 229 (2018) 121–129.
[60] R. Wang, X. Zhang, F. Li, et al., J. Energy Chem. 27 (2018) 343–350.
[61] Z. Wang, Y. Zhao, Y. Zhou, et al., Chem. Eng. J. 427 (2022) 131972.
[62] L. Xia, Z. Sun, Y. Wu, et al., Chem. Eng. J. 439 (2022) 135668.
[63] M.L. Chang, Z.M. Pan, D.D. Zheng, et al., ChemSusChem 16 (2023) e202202255.
[64] D. Zheng, Q. Wang, Z. Pan, et al., Sci. China Mater. 67 (2024) 1900–1906.
[65] Y. Shiraishi, T. Takii, T. Hagi, et al., Nat. Mater. 18 (2019) 985–993.
[66] W. Si, F. Haydous, U. Babic, et al., ACS Appl. Energy Mater. 2 (2019) 5438–5445.
[67] F. Li, X. Yue, D. Zhang, et al., Appl. Catal. B 292 (2021) 120179.